Nuclear Engineering and Technology 56 (2024) 2292–2306

Contents lists available at ScienceDirect

Nuclear Engineering and Technology

journal homepage: www.elsevier.com/locate/net

Original Article

Fracture analysis for nozzle cracks in nuclear reactor pressure vessel using FCPAS

Abdurrezzak Boz, Oğuzhan Demir *

Department of Mechanical Engineering, Bilecik Seyh Edebali University, 11230, Bilecik, Turkey

ARTICLE INFO

Keywords:
Fracture analysis
Stress intensity factors
Reactor pressure vessel
Nozzle cracks
Deflected cracks
Inclined cracks

ABSTRACT

This study addresses cracks and fracture problems in engineering structures that may cause significant challenges and safety concerns, with a focus on pressure vessels in nuclear power plants. Comprehensive parametric three-dimensional mixed mode fracture analyses for inclined and deflected nozzle corner cracks with various crack shape aspect ratios and depth ratios in nuclear reactor pressure vessels are carried out. Stress intensity factor (SIF) solutions are obtained using FRAC3D, which is part of Fracture and Crack Propagation Analysis System (FCPAS), employing enriched finite elements along the crack front. Also, improved empirical equations are developed to allow the determination of mixed mode SIFs, K_I, K_{II}, and K_{III}, for any values of the parameters considered in the study. This study provides practical solutions to assess the remaining life and fail-safe conditions of nuclear reactors by providing accurate SIF determination.

1. Introduction

In many engineering structures and industrial applications, cracks or fracture problems are encountered, and in some critical structures that require high technology and significant research and development expenditures, these failure types may become extremely vital. In a damaged structure, cracks may remain up to a certain safe size or a sudden fracture may cause serious financial losses, lead to dangerous accidents, and in some cases even cause loss of life. In computational fracture mechanics, numerical investigation of structures containing cracks requires an accurate and precise computation of fracture parameters to prevent such hazards and to ensure that damaged parts function safely i.e., to assess their remaining life/fail-safe conditions. Therefore, recent studies on ensuring the safe operation of damaged structures have become more important.

The reactor pressure vessel (RPV) is a key component of nuclear power plants along with the reactor core since, it is the heart of the nuclear steam supply system and is the penultimate safety fence to the release of radioactivity from the reactor core to the environment in case of a catastrophic failure [1,2]. Therefore, the structural integrity of RPV must be assured and maintained during operation. The number of studies on the investigation of fracture behavior of RPVs to ensure their safety increased significantly with the application of fracture mechanics approaches after 1960s. The effect of crack size on mode-I SIF was investigated experimentally for nozzle corner cracks by several researchers performing the burst test on epoxy models [3] and using the frozen-stress photo elastic technique [4–7]. Approximate stress intensity factor solutions [8–13] and numerical investigations using finite element method were also performed for nozzle corner cracks [14–31]. Most of the studies reported in the literature mainly concern pure mode-I fracture and crack growth problems dealing with the fatigue cracks initiated in the nozzles where a high-stress concentration occurs. However, in practice, many engineering structures containing cracks are exposed to various multi-axial loads i.e., the load directions are not perpendicular to the crack plane. Such loads are called mixed mode loads, under which crack may propagate in an inclined or deflected pattern from its actual plane. The existing developed approaches related to mode-I analysis are insufficient for these kinds of problems. Zhang et al. [32] analyzed cracks with different orientations using finite element alternating method in the reactor pressure vessel head penetration nozzles. They noted that the resulting mode-II and mode-III SIFs were dominant for some cracks and although their magnitudes were not large, they were not negligible. Spencer et al. [33] reported mixed mode SIF solutions obtained for two inclined cracks located at the inner surface of the RPV to show an initial demonstration of the usage of Grizzly which is a finite element-based simulation code. Liu et al. [34,35] performed mixed mode crack growth analyses for RPV under different loading conditions. FRANC3D software developed by a fracture group at

* Corresponding author.
E-mail address: oguzhan.demir@bilecik.edu.tr (O. Demir).

https://doi.org/10.1016/j.net.2024.01.040
Received 26 September 2023; Received in revised form 5 January 2024; Accepted 25 January 2024
Available online 5 February 2024

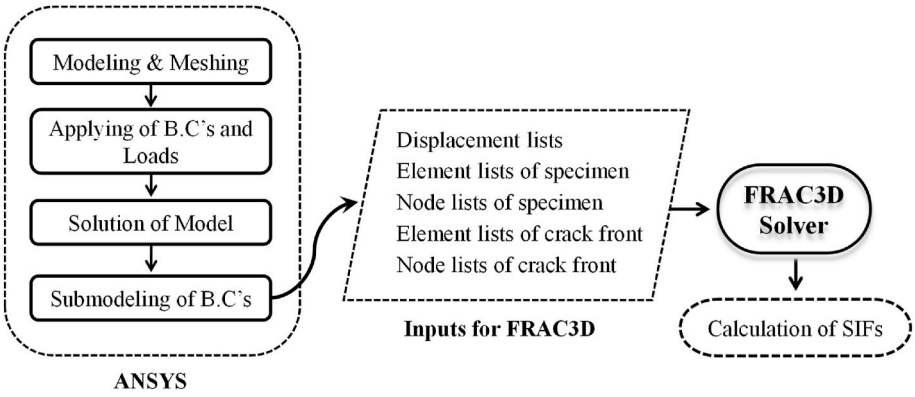

Fig. 1. The process map of the analysis procedure.

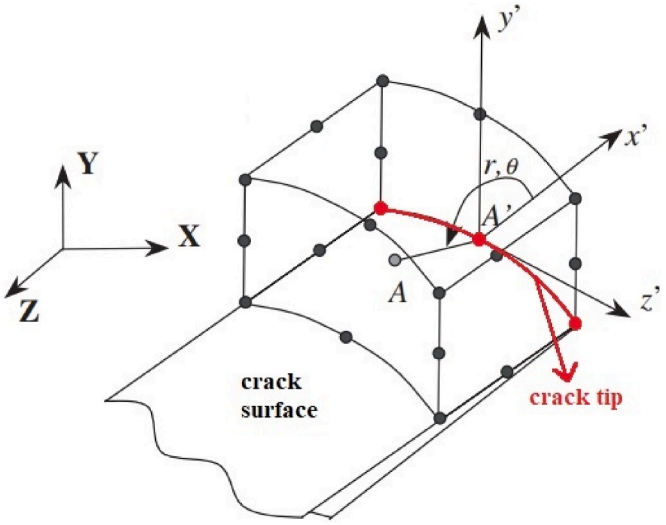

Fig. 2. Quadratic hexahedral enriched finite element touching the three-dimensional crack front [45].

Cornell University was used to compute SIFs and the sub-model technique was employed for crack propagation analyses [34,35]. It is indicated in these studies that the proportions of K_I, K_{II}, and K_{III} SIFs along the surface corner crack affect the direction of crack extension and, therefore the crack front shape. In previous studies [36–41], mixed mode-I/II, I/III and I/II/III fracture tests were performed for different types of specimens (compact tension shear- CTS specimen, T-specimen and compact tension-shearing and tearing- CTST specimen) under different mode mixity loading conditions. The results from mixed mode-I/II tests showed that although there is no mode-III external loading, mod-III SIF is also observed along the crack front due to Poisson's ratio effect of the material. The results for mixed mode-I/III tests also showed that although the applied load type is mixed mode-I/III, due to the out-of-plane bending effect, mode-II SIF is also observed in addition to mode-I and mode-III SIFs. Hence, mixed mode fracture behavior is complicated and includes some difficulties due to coupling of the in-plane shearing (mode-II) and out-of-plane tearing (mode-III) modes. Many problems related to engineering structures and machine parts seen in practice involve three dimensional nature. In order to ensure the safety of RPV, three-dimensional modeling capabilities and solutions, which are relatively limited in the literature for thorough understanding and clarification of mixed mode fracture conditions on RPV, are required for designing more reliable reactors. Due to the complexity of the configuration and of the stress distribution around nozzle junction, detailed investigation of mixed mode fracture behavior is needed.

A numerical assessment of damaged structures containing cracks requires an accurate and precise solution of three-dimensional SIFs, i.e., K_I, K_{II}, and K_{III} along the crack front which has a remarkable role on mixed mode fracture analysis. The RPV serves as the central component of these plants, acting as the nucleus of the nuclear steam supply system and serving as a crucial safety barrier to prevent the release of radioactivity in the event of a catastrophic failure. The potential for cracks or fractures in the RPV poses a significant risk, with the capacity to lead to severe financial losses, hazardous accidents, and, in extreme cases, loss of life. The mixed mode loads, where the directions are not perpendicular to the crack plane, result in crack propagation in inclined or deflected patterns, presenting a challenge not adequately addressed by current approaches. In this study, comprehensive and parametric fracture analyses of a wide range of inclined and deflected nozzle corner cracks with different aspect ratios and depth values for RPV are presented in detail to gain a deeper understanding of mixed mode fracture conditions in RPVs. Moreover, recognizing the lack of comprehensive empirical equations for predicting K_I, K_{II}, and K_{III} SIFs for any crack shape and orientation in RPVs, based on the numerical results obtained for the in-depth cases aforementioned, improved regression-based empirical equations have been proposed. These equations aim to provide accurate predictions of SIFs, enhancing the practical applicability of the study's findings in the field of nuclear power plant engineering.

2. Computation of mixed mode SIFs

Details related to modeling and fracture analysis procedures are briefly described in this section. The process steps for the analysis procedure are shown in Fig. 1. ANSYS™ [42] is used for modeling and the solution of the problem involving the whole assembly. After performing the stress analysis, the element, node lists connected to crack front and the sub-model, and displacement lists belonging to contact surfaces of the sub-model are taken from ANSYS. Those data are used in FRAC3D solver to compute SIFs along the crack front. FRAC3D solver [43,44], which is a general-purpose, standalone program employing enriched finite elements in an effort to compute three-dimensional mixed mode SIFs and is the main part of Fracture and Crack Propagation Analysis System (FCPAS) is used for fracture analyses. The enriched finite elements permit direct computation of SIFs with no pre- and post-process interventions and without the need a special techniques or procedures near the crack front and additional treatments after solution of the finite element analysis. The crack front is surrounded by enriched elements sharing an edge or point. A representative view of a quadratic hexahedral enriched finite element touching the three-dimensional crack front is shown in Fig. 2. The SIFs and displacements along the crack front can be computed concurrently since these elements also include the unknown SIFs into finite element formulation in addition to nodal displacements and shape functions (Eq. (1)). Details regarding with finite

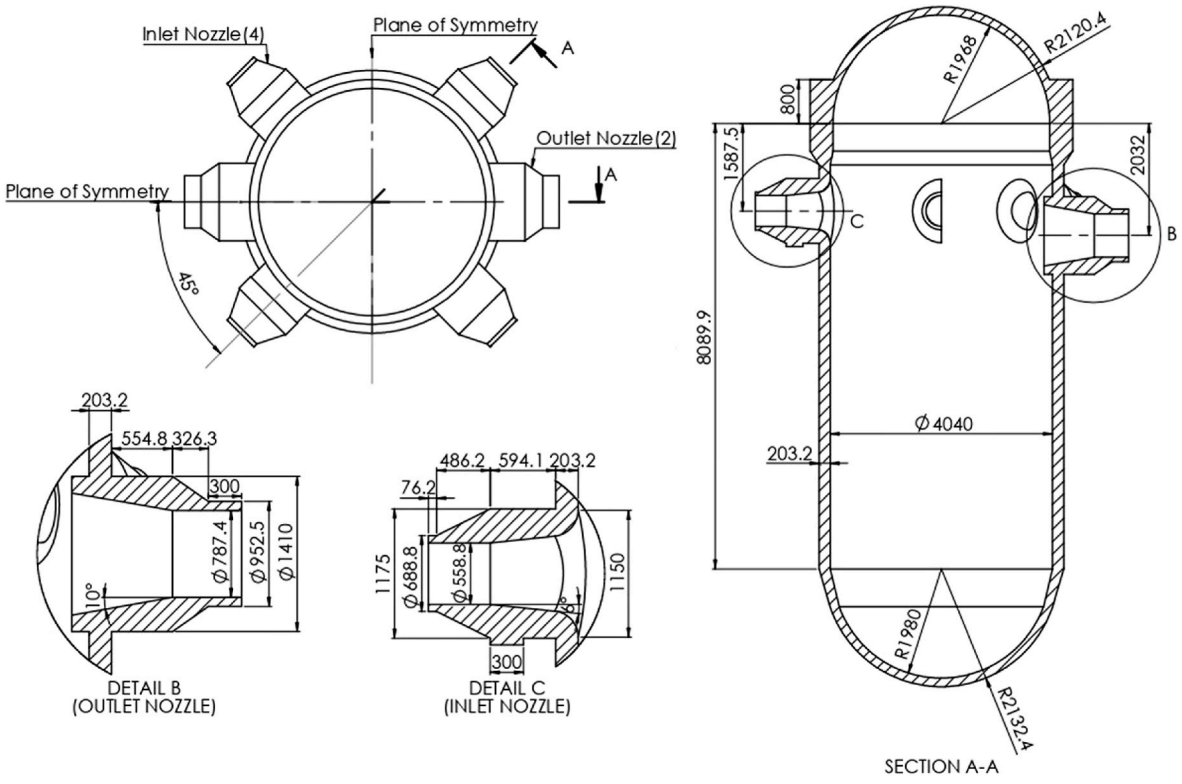

Fig. 3. Detailed dimensions of the AP1000 RPV model [46].

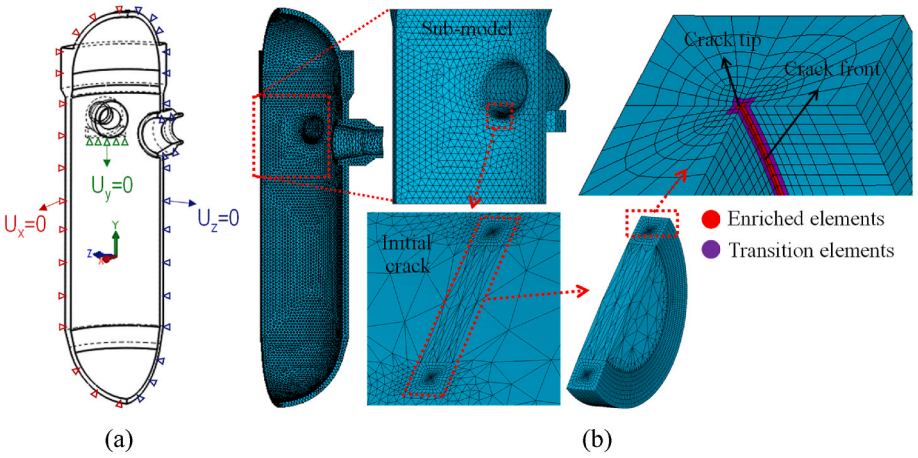

Fig. 4. The RPV model used in the analyses, (a) boundary conditions, (b) close-up view of the initial crack region including enriched and transition elements.

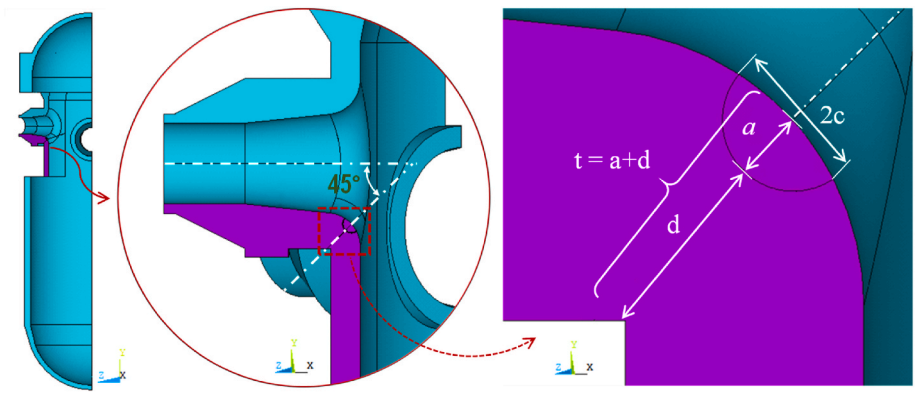

Fig. 5. Details of nozzle corner crack.

element formulations and numerical integration of the enriched elements can be found in Refs. [43,44].

$$u(\xi,\eta,\rho)=\sum_{j=1}^{m}N_j(\xi,\eta,\rho)u_j+Z_0(\xi,\eta,\rho)\left(f_u(\xi,\eta,\rho)-\sum_{j=1}^{m}N_j(\xi,\eta,\rho)f_{uj}\right)\left(\sum_{i=1}^{ntip}N_i(\Gamma)K_I^i\right)$$
$$+Z_0(\xi,\eta,\rho)\left(g_u(\xi,\eta,\rho)-\sum_{j=1}^{m}N_j(\xi,\eta,\rho)g_{uj}\right)\left(\sum_{i=1}^{ntip}N_i(\Gamma)K_{II}^i\right)$$
$$+Z_0(\xi,\eta,\rho)\left(h_u(\xi,\eta,\rho)-\sum_{j=1}^{m}N_j(\xi,\eta,\rho)h_{uj}\right)\left(\sum_{i=1}^{ntip}N_i(\Gamma)K_{III}^i\right) \quad (1)$$

Calculation of stiffness matrices of enriched elements contains derivatives of the above displacement fields. The stress intensity factors are directly embedded in the enriched element formulation and thus, they are computed automatically using FRAC3D without any post-processing. In Eq. (1), u_j are the m unknown nodal displacements, ξ, η and ρ are the local coordinates in the enriched elements and N_j are the regular finite element shape functions. Z_0 is a zeroing function that is 1 for all enriched elements and varies between 0 and 1, m is 20 or 10 depends on element type, and f_u, g_u and h_u are obtained from the analytically known functions in the asymptotic crack tip displacement expressions for mode-I, –II and –III displacement components. K_I^i, K_{II}^i and K_{III}^i are the unknown nodal stress intensity factors at the ith crack front node, and the series ($\sum_{i=1}^{ntip}N_i(\Gamma)K_I^i$, K_{II}^i and K_{III}^i) symbolizes the stress intensity factor variations along the whole crack front within the element shown and the neighboring nodes on the crack front. *ntip* is number of nodes on the edge of one element along the crack front and is 3 for a quadratic enriched element. The local isoparametric coordinate, Γ varies between - 1 and 1.

Table 1
Geometric parameters utilized in sensitivity analyses.

Parameters	Values
Crack depth ratio (a/t)	0.0625; 0.125; 0.25
Crack shape aspect ratio (a/c)	0.5; 1.0; 2.0
Crack inclination angle (β)	**0°**; 15°; 30°; **45°**; 60°; 75°; **90°**
Crack deflection angle (α)	0°; 15°; 30°; 45°; 60°; 75°

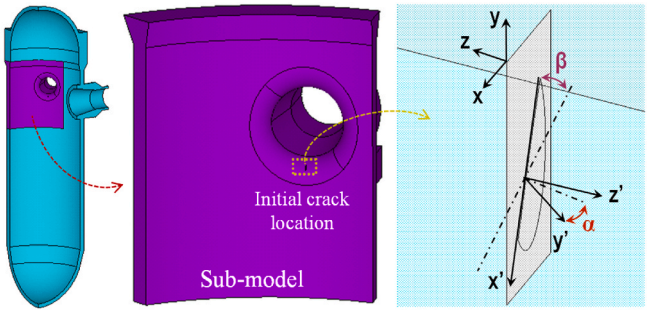

Fig. 6. Detailed view of the initial crack located on the sub-model.

3. Problem description

In this section, details of three-dimensional mixed mode surface crack problem are depicted for the AP1000 RPV which has a third-generation advanced passive cooling system with four in-let and two out-let nozzles. A comparison is first done in this section to validate the applied three-dimensional enriched element method. Liu et al. [35] analyzed this problem to investigate the effect of thermal stress on crack propagation. The SIF solutions given for different inclination angles (β) in Ref. [35] are compared in the current study to validate the method. Since the AP1000 reactor pressure vessel has symmetry in two axes, it is modeled as a quarter model to simplify the problem. In Fig. 3, the geometric details of the model are summarized. The material considered for the analyses is SA508 Gr.3 Cl.1 steel. Young's modulus and Poisson's ratio of the material are 186 GPa and 0.3, respectively. The finite element model used in the fracture analyses and the close-up view of the initial crack region including enriched and transition elements are shown in Fig. 4. The internal pressure of 17.13 MPa is applied on the inner surface as is the case with the study performed by Liu et al. [35] to compare the analysis results for some specific loading conditions. Fig. 5 depicts a surface corner crack at the inlet nozzle-cylinder intersection area of RPV. "a" is the crack depth, "2c" is the crack length, and "t"

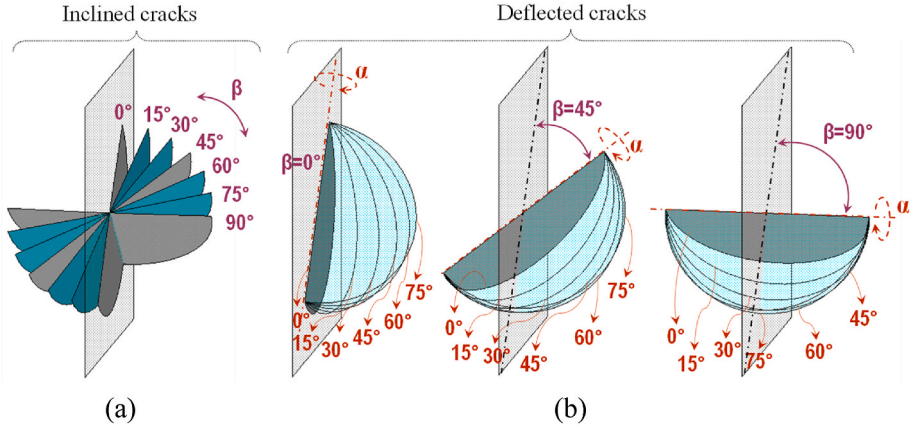

Fig. 7. (a) Inclined crack, (b) deflected crack cases considered in the study.

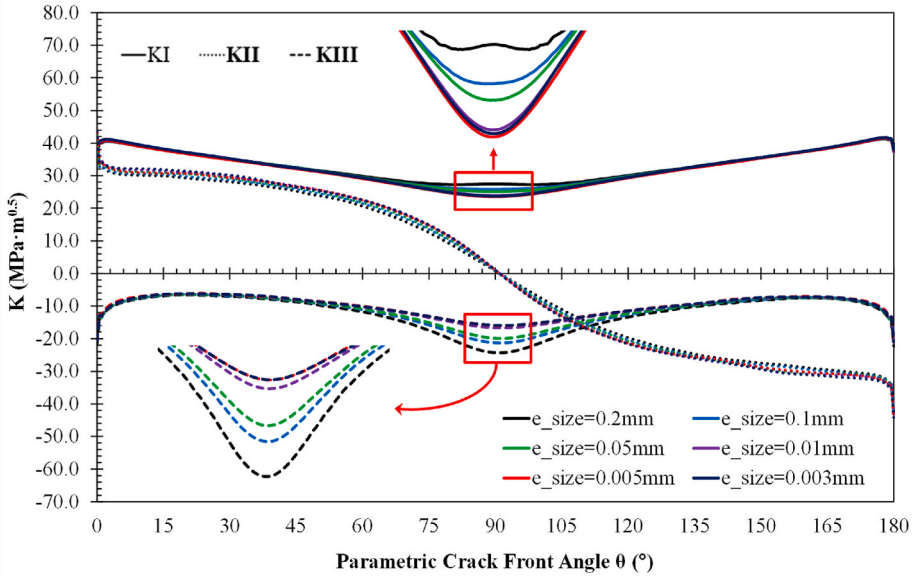

Fig. 8. Mixed mode SIF distributions along the crack front obtained for different crack tip element sizes for the case; α = 0°, β = 45°, a/t = 0.125 and a/c = 2.0.

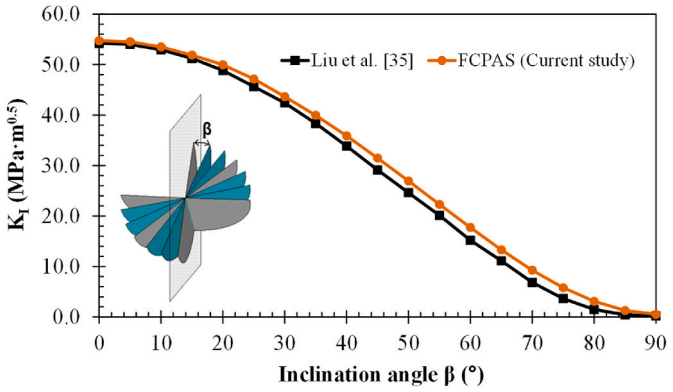

Fig. 9. Comparison of mode-I SIFs obtained from the current study by FCPAS and from the reference study [35].

represents the nozzle section thickness including crack depth in a direction oriented 45-degrees from the center of the inner surface to the outer surface, as shown in Fig. 5. The value of "t" is approximately 240 mm. To perform a large spectrum of SIF solutions and determine their sensitivity to the specified variables, the geometric parameters listed in Table 1 are utilized to cover all possible combinations. However, there might be some special cases ineligible for analysis such as some points of the crack surface extending beyond the nozzle surface. In Fig. 6, a detailed view of the surface corner crack located at the inlet nozzle-cylinder intersection on the sub-model is presented. In the case of an inclined crack, the crack plane is rotated with respect to the local *y'* axis by *β* for which axis representations are given in Fig. 6. In the case of a deflected crack, the crack plane is rotated with respect to the local *x'* axis by *α*. The inclination and deflection angles are measured from a plane parallel to the local x–y plane. Fig. 7 illustrates the cases of deflected and inclined cracks considered in the study.

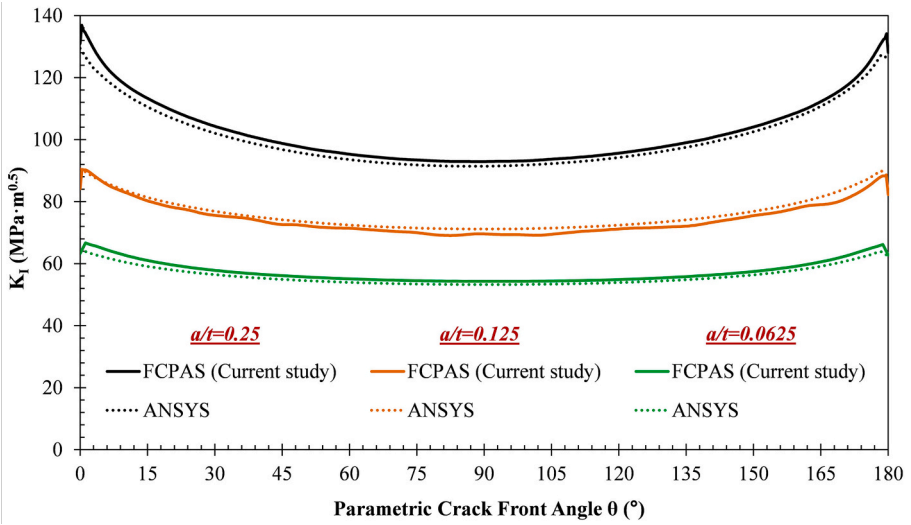

Fig. 10. The mode-I SIF distributions for different crack depth ratio obtained by FCPAS and Ansys for the case; α = β = 0° and a/c = 1.0.

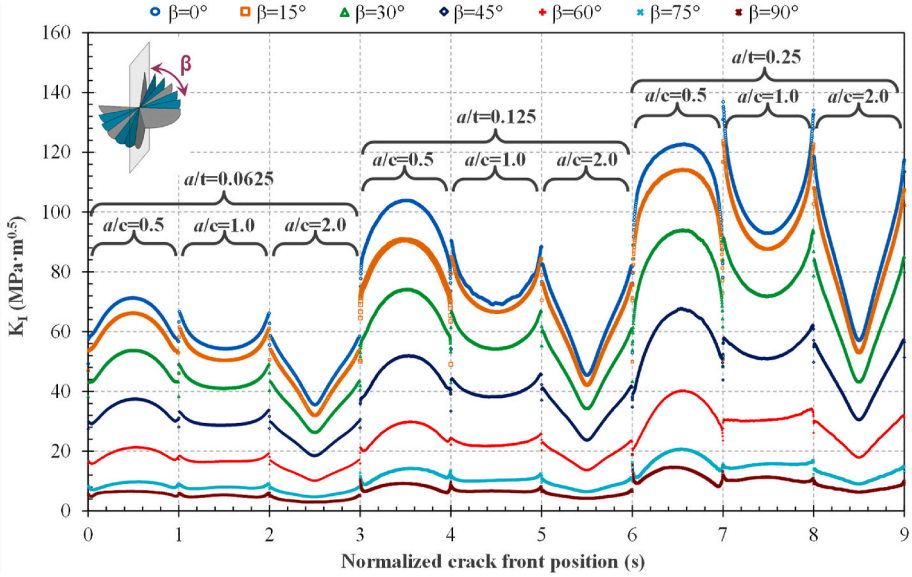

Fig. 11. Comparisons of mode-I SIF distributions for inclined cracks.

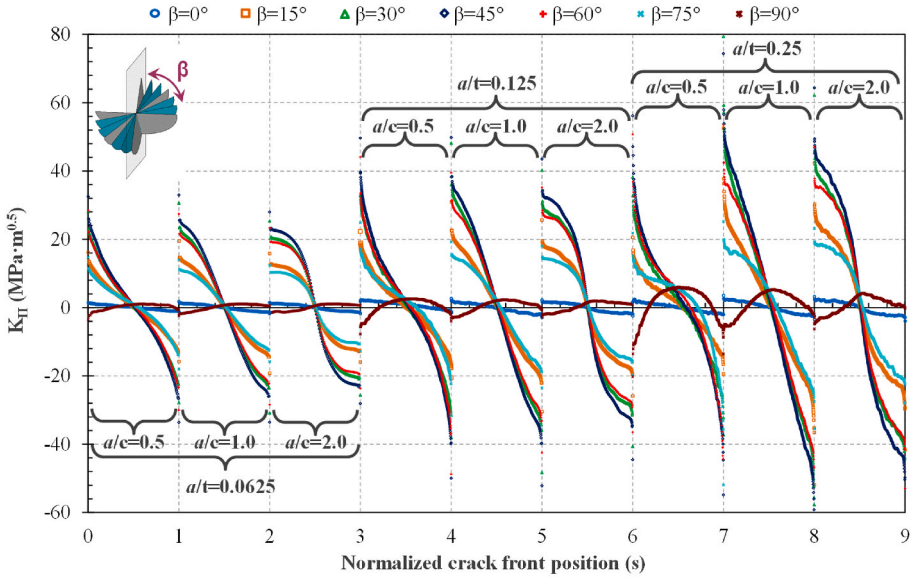

Fig. 12. Comparisons of mode-II SIF distributions for inclined cracks.

4. Numerical results

To achieve the optimum mesh structures and accurate and exact analysis results, a series of mesh sensitivity analyses are carried out. In this context, the edge size of the enriched elements located at the crack tip is systematically reduced, and then the obtained SIFs along the crack front are compared. In Fig. 8, a comparison of the mixed mode SIF distributions along the crack front obtained for different crack tip element sizes is plotted for the case; $\alpha = 0°$, $\beta = 45°$, $a/t = 0.125$, $a/c = 2.0$. As can be observed from the figure, the K_I, K_{II}, and K_{III} SIF distributions converge when the element size ranges from 0.005 mm to 0.003 mm. The two SIF solutions are almost identical. Therefore, the enriched element size of 0.005 mm is deemed suitable for the analyses. The mode-I SIF solutions given for the case; $a/t = 0.0625$, $a/c = 1.0$, for different inclination angles (β) in the study performed by Liu et al. [35] are compared in Fig. 9 to validate the applied three-dimensional enriched element method. The comparison results demonstrate that there is a very good agreement between the results of this study and those of application example. As a second validation case, fracture analyses performed for different crack depth ratios ($\alpha = \beta = 0°$, $a/c = 1.0$) using Ansys and comparison of mode-I SIF variations are given in Fig. 10. As is seen that similar tendencies are observed for both software. In this section, detailed three-dimensional mixed mode SIF solutions are introduced including all possible combinations of the crack shape and patterns listed in Table 1. It should be noted that all comparison graphs (Figs. 11–22) exhibited in this section contain SIF distributions for a combination of 9 cases under 3 different values of crack shape aspect ratio (a/c), and crack depth ratio (a/t). Therefore in these figures (Figs. 11–22), the normalized crack front position on x-axis changes between 0 and 9.

4.1. Fracture analyses for inclined cracks

First, SIF solutions are provided for inclined cracks (Fig. 7-a). Fig. 11 shows the comparison of mode-I SIF distributions along the crack fronts for different inclined cracks including all possible crack aspect ratios and

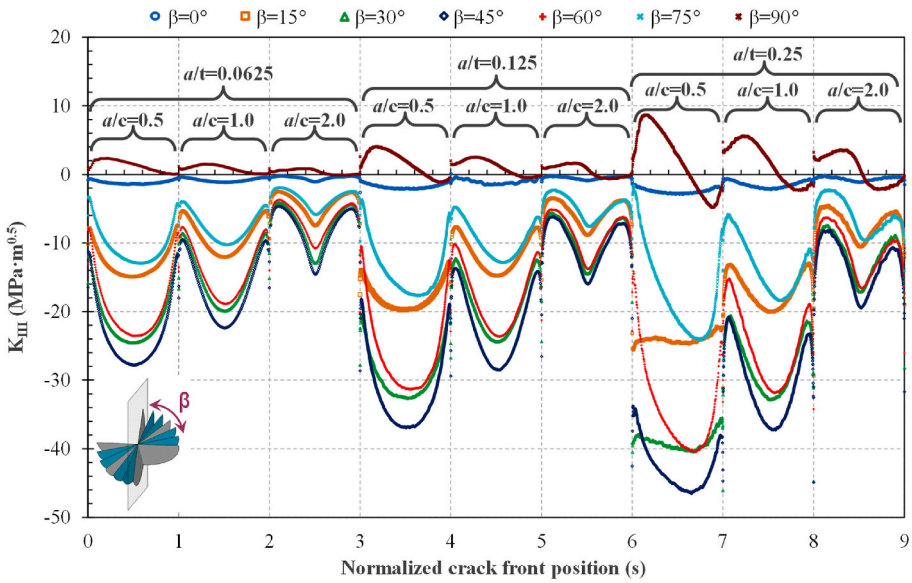

Fig. 13. Comparisons of mode-III SIF distributions for inclined cracks.

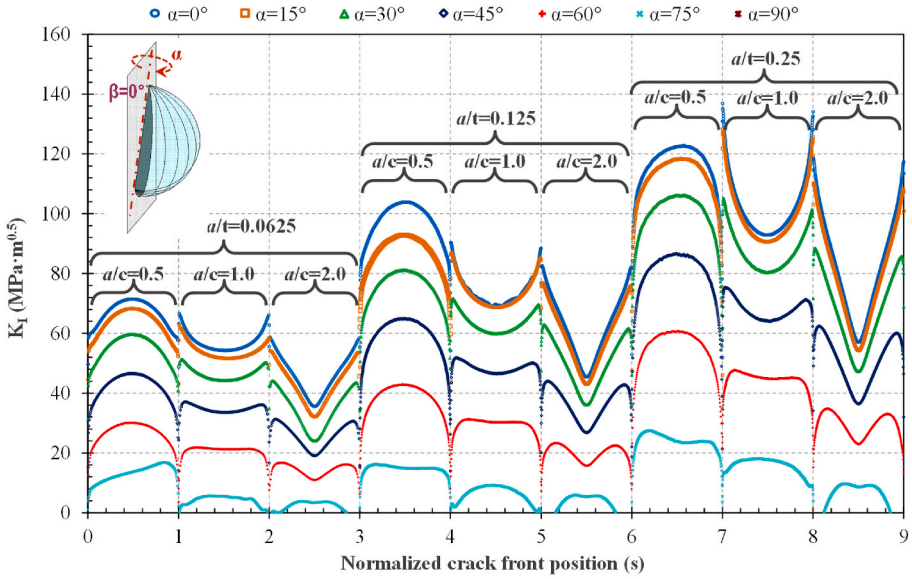

Fig. 14. Comparisons of mode-I SIF distributions for deflected cracks (β = 0°).

crack depths listed in Table 1. It should be indicated that each interval on the horizontal axis represents the distribution of SIFs along the crack front for each crack configuration considered. It is observed from the figure that, for a given crack aspect ratio, a/c, as the crack depth ratio (a/t) increases i.e., the initial crack approaches the boundary surface, due to the back surface effect, the mode-I SIFs increase for each crack configuration. This so-called back surface effect is caused due to the decreased rigidity of the ligament between the crack and back surface. Also, for a given a/c, the amount of increment of SIF value is proportional with a/t, i.e., the increment amount is maximum for a/c = 0.5, minimum for a/c = 2.0. The value of mode-I SIF along the whole crack front is maximum for the case that the crack is not inclined, i.e., β = 0, and consistently decreases with increasing inclination angle. Furthermore, for crack aspect ratios with a/c = 0.50, the maximum SIF is observed in the deepest region. For a/c = 1.0 and 2.0, on the contrary, the SIFs near the free surface locations are higher than at the center of the crack depth. Another conclusion from the curves is that, for a given a/t, K_I decreases with increasing a/c ratios. A comparison of mode-II SIF distributions along the crack fronts for different inclined cracks is included in Fig. 12. It is clearly seen that, for the intermediate angles, K_{II} has its maximum value at the free-surface points and its distribution is nearly linear and anti-symmetric. Also, for β = 0° and 90° cases and for a/t = 0.0625, the magnitude of K_{II} is close to zero along the whole crack front for all a/c ratios, while gradually increases in magnitude with increasing a/t. Another observation is that, as inclination angle increases, K_{II} progressively increases until it reaches its maximum magnitude at β = 45°, and decreases as the inclination angle further increases. Finally, for the intermediate angles, the increment of K_{II} with increasing a/t ratios for a given a/c is also seen. Fig. 13 shows the comparison of mode-III SIF distributions along the crack fronts for different inclined cracks. Similar to the behavior of K_{II}, for all crack configurations, K_{III} gradually increases in magnitude as inclination angle increases, reaching its maximum magnitude at β = 45°, and decreases as the inclination angle further increases. It is clearly observed that, for a given a/t, K_{III} decreases with increasing a/c ratios, and for a given a/c, on the contrary, K_{III} increases with increasing a/t ratios. It should be

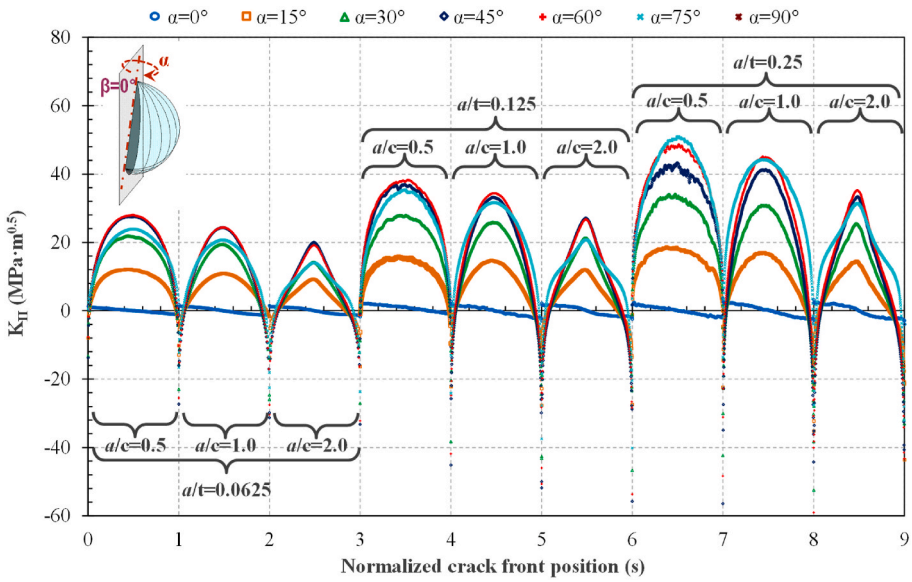

Fig. 15. Comparisons of mode-II SIF distributions for deflected cracks (β = 0°).

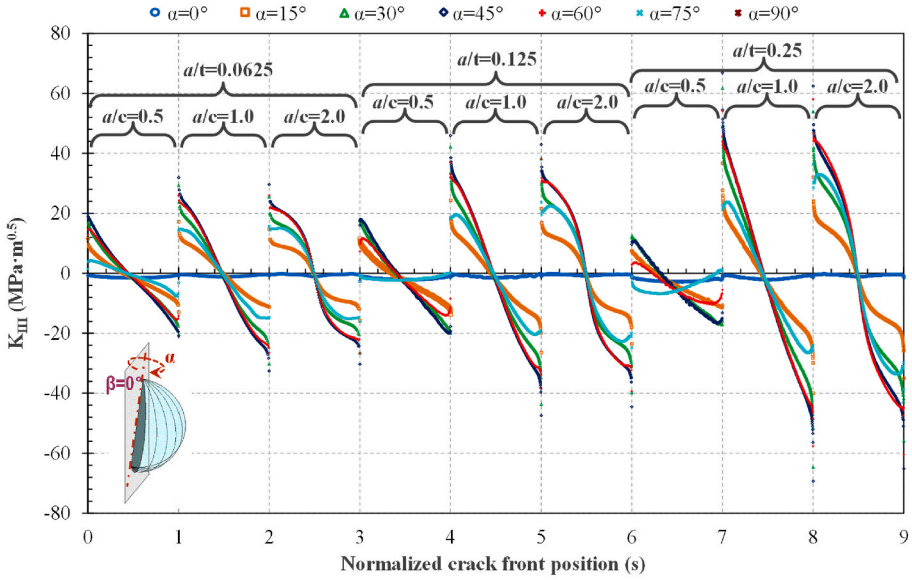

Fig. 16. Comparisons of mode-III SIF distributions for deflected cracks (β = 0°).

noted that in this paper, the terms "increase" and "decrease" are used in the magnitudes, not necessarily in terms of the algebraic sense. Similar to the behavior of K_{II}, for β = 0° and 90° cases and for $a/t = 0.0625$, K_{III} is nearly zero along the crack front, and increases with increasing a/t. For the intermediate angles, the maximum K_{III} occurs at the deepest point and as a/t ratio increases the level of asymmetry increases.

4.2. Fracture analyses for deflected cracks ($\beta = 0°$)

In this sub-section, results of fracture analyses are presented for deflected cracks for the case of β = 0° (Fig. 7-b). In Fig. 14, variations of mode-I SIFs along the crack fronts for different deflected cracks (β = 0°) with various crack shapes listed in Table 1 is presented. As is the case with the inclined cracks, due to the back surface effect, the increased K_I with increasing the crack depth ratio (a/t) is apparently observed for each crack shape, and also the amount of increment of K_I is proportional with a/c. K_I is maximum for α = 0°, and progressively decreases in distribution of K_I with increasing deflection angle as expected, and its magnitudes are partially below zero for α = 75° and completely below zero for α = 90°, indicating the crack surface contact. Similar to the behavior of inclined cracks, the deepest point has the maximum SIF for the case of $a/c = 0.50$. Conversely, for $a/c = 1.0$ and 2.0, SIFs near the free surface points are maximum, and for a given a/t, the decreased K_I as the ratio, a/c, further increases is explicitly seen. Similarly, distributions of mode-II and –III SIFs along the crack fronts for deflected cracks for the case of β = 0° are presented in Figs. 15 and 16, respectively. SIF distributions for α = 90° are not included in these figures due to their magnitude is completely below zero. As evident from the figures, the behavior of mode-II SIFs (Fig. 15) closely resembles the behavior of mode-III given in Fig. 13, while mode-III SIF distributions (Fig. 16) show a similar tendency to the mode-II SIF distributions shown in Fig. 14.

4.3. Fracture analyses for deflected cracks ($\beta = 45°$)

SIF solutions for deflected cracks for the case of β = 45° are presented in this sub-section. Fig. 17 illustrates the distributions of mode-I SIFs

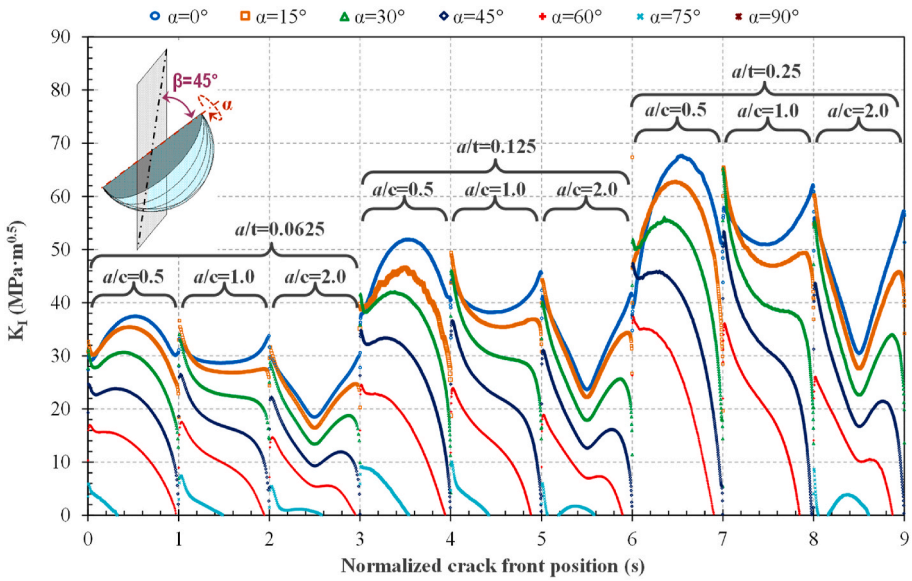

Fig. 17. Comparisons of mode-I SIF distributions for deflected cracks (β = 45°).

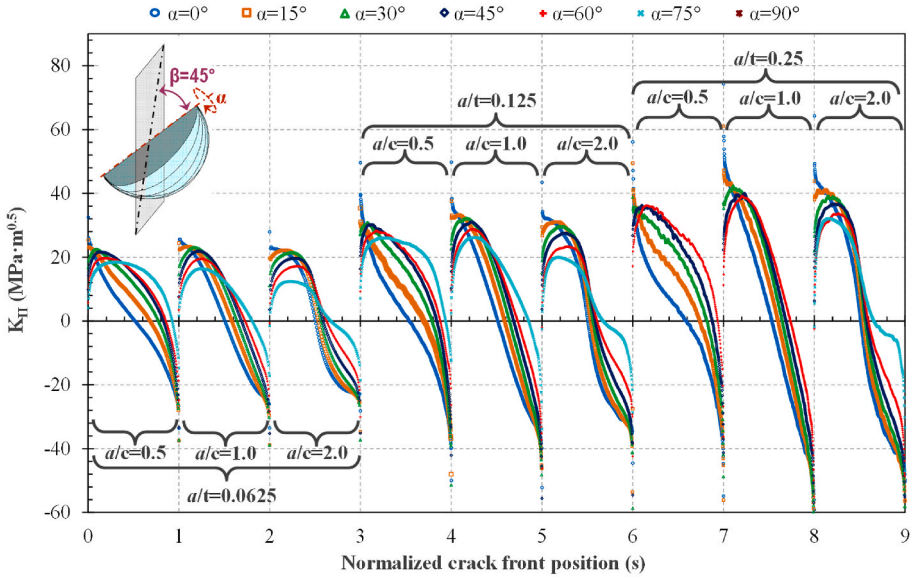

Fig. 18. Comparisons of mode-II SIF distributions for deflected cracks (β = 45°).

along the crack fronts for the case of deflected cracks (β = 45°) with different crack configurations listed in Table 1. As is seen, K_I distributions closely resemble the behavior of K_I presented in Fig. 14 for the previous case, except for the increasing level of asymmetry with increasing crack deflection angle and crack depth ratio. It should be noted that some cases for α = 75° and completely for α = 90° are not included in the figure. As mentioned above some cases are ineligible for analysis due to modeling problems of the initial crack related to crack shape such as some points of the crack surface extending beyond the nozzle surface. Variations of K_{II} along the deflected crack fronts for β = 45° with different crack shapes are represented in Fig. 18. As is the case with Fig. 12 given for K_{II} distributions for inclined cracks, a similar tendency is observed for each crack configuration, except asymmetric distribution is present apparently, and also the magnitudes of K_{II} are out of zero for α = 0°. Fig. 19 shows the distributions of mode-III SIFs for deflected cracks (β = 45°) with different shape ratios. A high level of asymmetry compared to previous figures plotted for K_{III} variations is clearly seen.

4.4. Fracture analyses for deflected cracks (β = 90°)

Finally, results of fracture analyses are presented for deflected cracks (β = 90°) with different crack configurations listed in Table 1. In Figs. 20–22, SIF distributions along the crack fronts are given. It is seen from Figs. 20–22 that, compared to results of the other crack configurations, the almost lowest SIF values are obtained for all three fracture modes under the same a/t and a/c ratios and the magnitudes of resultant K_I values are relatively close to K_{II} and K_{III} SIFs. The problem is further mixed-mode compared to other cases and complicated for modeling of the initial crack. Therefore, SIF solutions for α = 60°, 75° and 90° are not included in (Figs. 20–22) as modeling of these crack cases is not feasible or possible. Also, for α = 45°, K_I values are partially below zero (Fig. 20) which is physically impossible and reflects the crack surface contact.

5. Development of new mixed mode SIF equation

In an effort to establish the effect of a/t ratios, a/c ratios, crack

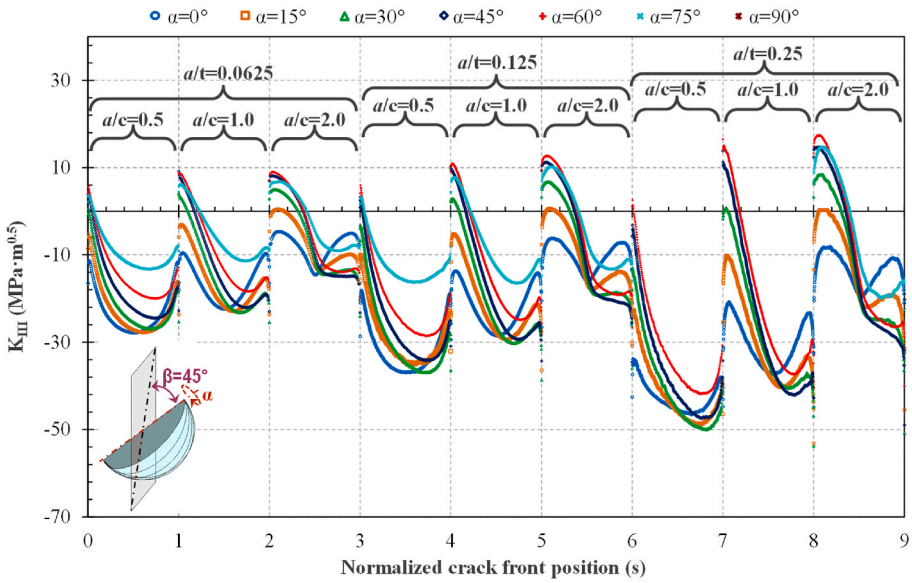

Fig. 19. Comparisons of mode-III SIF distributions for deflected cracks (β = 45°).

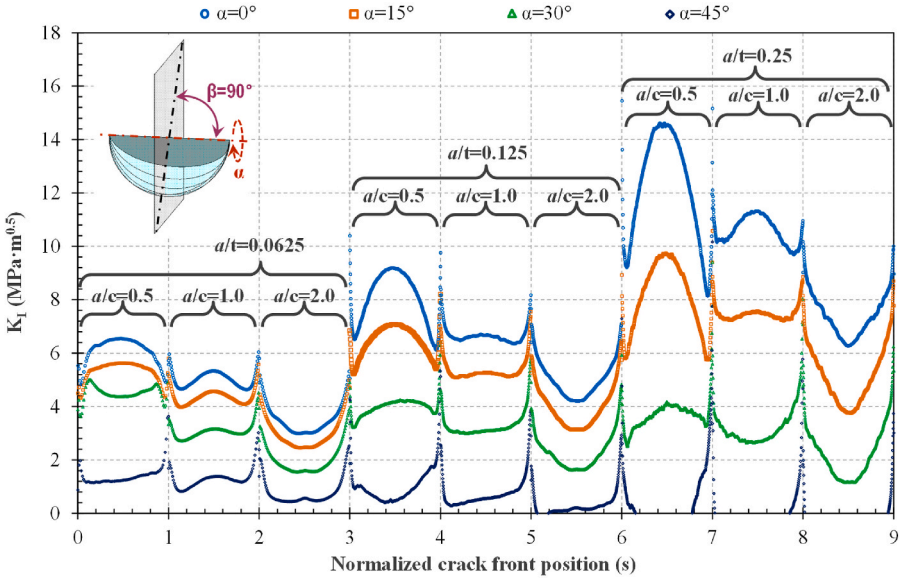

Fig. 20. Comparisons of mode-I SIF distributions for deflected cracks (β = 90°).

inclination (β), and deflection (α) angles on the resultant K_I, K_{II} and K_{III} SIFs obtained from all crack configurations considered in this study, main effects analyses are performed with the provided results of fracture analysis. The nozzle junction of RPV is subjected to higher and more complex stresses than the remaining parts due to the complexity of the construction. Therefore, a detailed investigation of three-dimensional mixed mode analysis is needed to understand the nature of fracture behavior and the effect of crack parameters on this complicated behavior for designing more reliable reactors. In order to summarize the effect of these crack parameters on mixed mode SIFs, additional comparison graphs are provided. In Figs. 23 and 24, comparisons of mean of K_I, K_{II} and K_{III} obtained for the depth point from all cases considered are represented as a function of inclination or deflection angles for the cracks with different a/t and a/c ratios, respectively. In Fig. 23, the mean of K_I, K_{II} and K_{III} refers to the average values of these SIFs computed for different a/c ratios under a given a/t ratio, crack inclination (β), and deflection (α) angles while it represents the average of SIFs obtained for different a/t under a given a/c, β, and α in Fig. 24. An obvious conclusion from both figures would be that the effect of a/t and a/c ratios on K_I is greatest for non-inclined/non-deflected cases (α = β = 0°) and decreases as inclination/deflection angles increase, whereas it is vice versa for K_{II}, i.e., a/t and a/c ratios have the least influence on K_{II} for α = β = 0°, and the influence increases mostly with increasing the inclination/deflection angles. Another observation from both figures is that for deflected cracks, the level of influence of a/t and a/c ratios on K_{III} generally does not change much with the variation of inclination angle.

Instead of time-consuming methods to determine SIFs, equations or criteria developed for customized problems are highly desirable in terms of practicality. There is a need for an improved equation considering the influence of the variables on analysis results, that can provide a practical method to determine mixed mode SIFs for intermediate values of the variables without the need for analysis. After determining the effects of parameters considered on mixed mode SIFs, regression-based [48] empirical equations are developed using K_I, K_{II}, and K_{III} values obtained from all SIF solutions presented above for the crack depth point. The SIFs

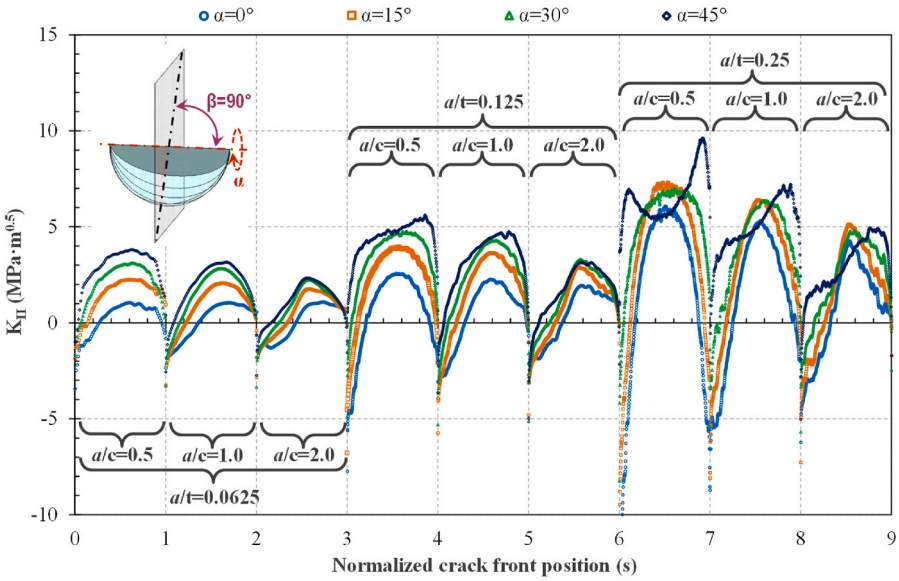

Fig. 21. Comparisons of mode-II SIF distributions for deflected cracks (β = 90°).

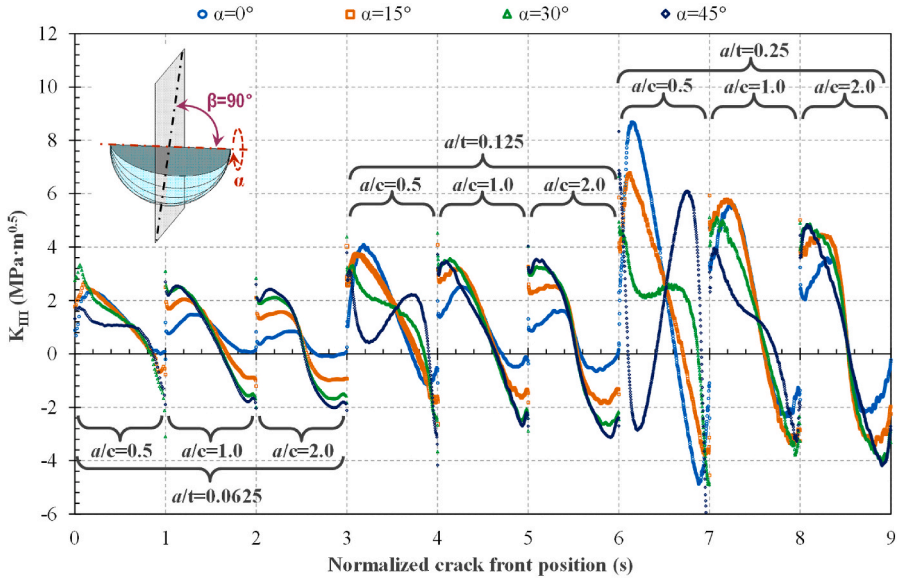

Fig. 22. Comparisons of mode-III SIF distributions for deflected cracks (β = 90°).

obtained for cases where K_I values are partially or completely negative have been excluded from the regression analysis. Poisson regression analysis is employed to develop an empirical equation to determine K_I. The equation is defined as follows;

$$K_I = e^{y} \tag{2}$$

where e is the Euler number, and y is expressed as follows;

$$y = 4.122 + 7.012\frac{a}{t} - 0.513\frac{a}{c} - 13.22\left(\frac{a}{t}\right)^2 - 0.99\beta^2 - 0.812\alpha^3 + 0.965\frac{a}{t}\alpha^2 - 0.133\frac{a}{c}\alpha^2 - 0.403\beta^2\alpha \tag{3}$$

In Eqs. (2) and (3), α and β in radian, K_I in MPam$^{0.5}$. To validate the developed empirical equation, the mode-I SIF solutions provided for cracks with various crack shape aspect ratios and depth ratios in the study conducted by Du and Shi [47] are compared in Fig. 25. It is evident that there is an excellent agreement between the results obtained from the equation and those from the reference study [47]. Thus, it can be concluded that Eq. (2) can effectively be employed to determine the mode-I SIF for any intermediate values of the parameters listed in Table 1. Finally, similar to the equation mentioned above, regression-based empirical equations are formulated for determining K_{II} and K_{III} SIFs, and they are presented below;

$$\begin{aligned} K_{II} = {} & -1.444 + 23.286\frac{a}{t} + 1.012\beta + 46.371\alpha - 66.660\left(\frac{a}{t}\right)^2 + 206.940\frac{a}{t}\alpha \\ & - 23.263\alpha^2 - 5.328\frac{a}{c}\alpha - 34.440\alpha\beta + 3.457\frac{a}{c}\beta\alpha + 69.244\left(\frac{a}{t}\right)^2\beta \\ & - 249.349\left(\frac{a}{t}\right)^2\alpha - 1.104\frac{a^3}{c^2t} - 2.415a^3 - 13.651\frac{a^2}{tc}\alpha - 4.363\frac{a}{t}\beta^2 \\ & - 72.828\frac{a}{t}\beta\alpha - 16.427\frac{a}{t}\alpha^2 + 1.493\beta^2\alpha + 18.932\beta\alpha^2 \end{aligned} \tag{4}$$

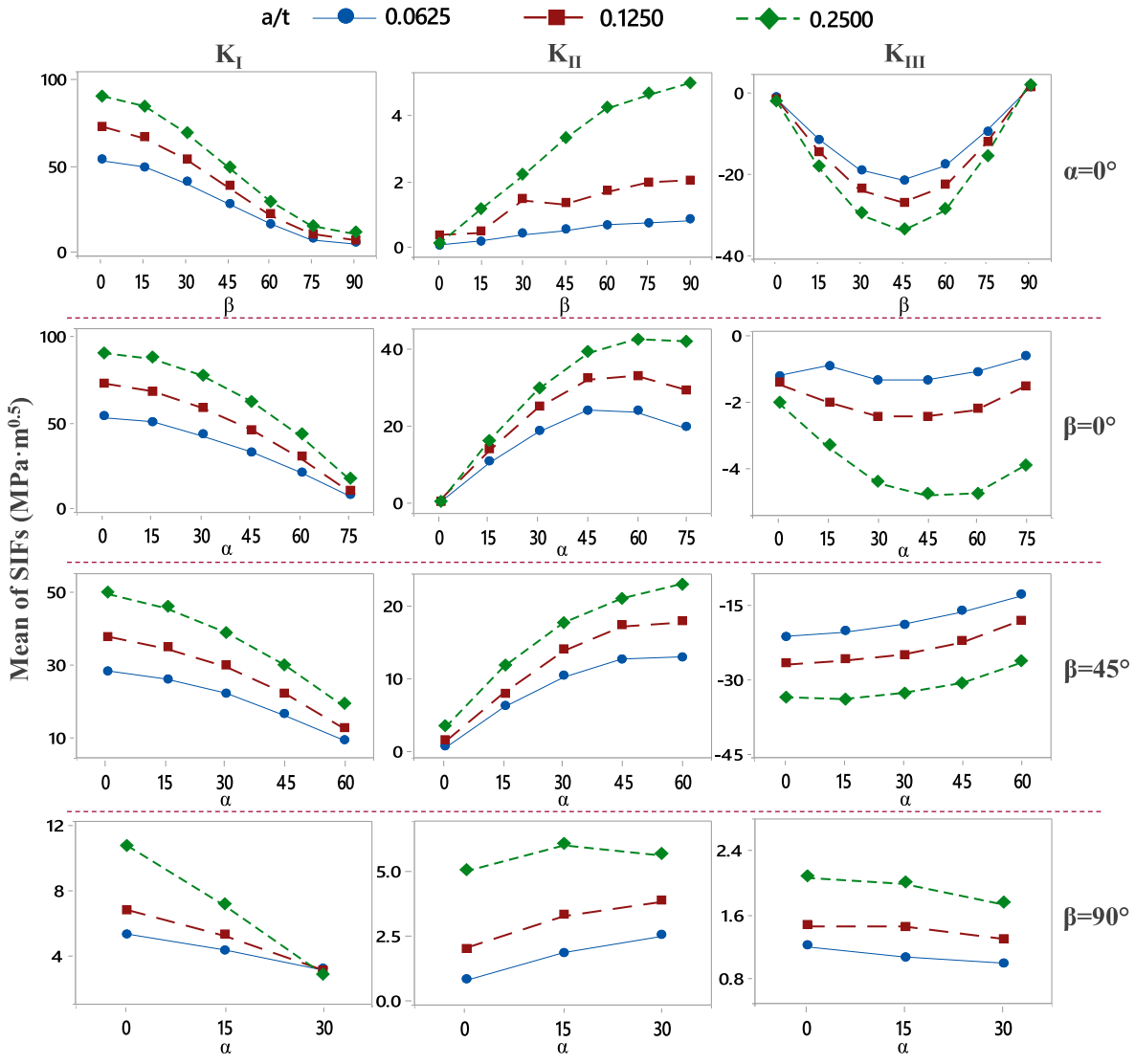

Fig. 23. Effect of crack depth ratio (a/t) on the resultant SIFs obtained from the all cases considered.

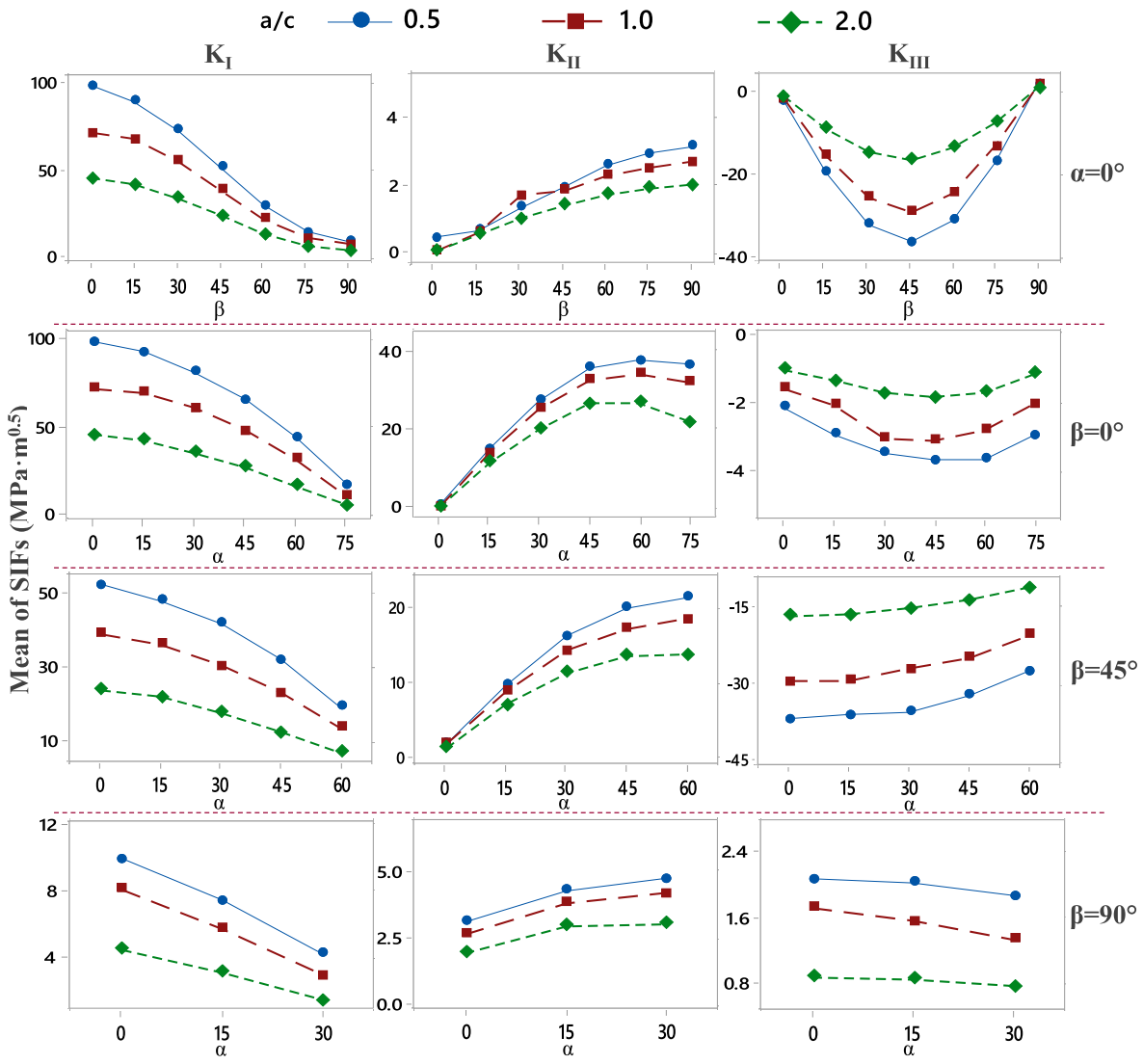

Fig. 24. Effect of crack shape aspect ratio (a/c) on the resultant SIFs obtained from the all cases considered.

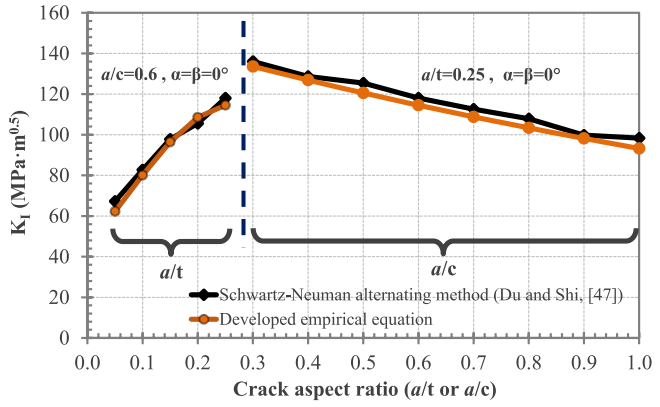

Fig. 25. Comparisons of mode-I SIFs obtained from the developed empirical equation and from the reference study [47] for different crack configurations.

$$K_{III} = 1.079 - 25.925\frac{a}{t} - 81.260\beta - 0.715\left(\frac{a}{c}\right)^2 + 53.095\beta^2 + 19.305\frac{a^2}{tc} + 30.728\frac{a}{c}\beta - 46.643\frac{a}{t}\alpha + 15.351\beta\alpha + 105.071\frac{a}{t}\beta^2 + 19.925\frac{a}{t}\beta\alpha - 159.751\frac{a}{t}\beta + 31.217\frac{a}{t}\alpha^2 - 20.152\frac{a}{c}\beta^2 - 10.563\beta^2\alpha \quad (5)$$

In order to demonstrate the applicability of the developed empirical Eqs. (4) and (5), an extended series of fracture analyses has been performed by FCPAS for different intermediate values of the parameters that have not been analyzed before, and the SIFs obtained from the empirical equations and FCPAS for the crack depth point are given in Table 2. Although for some cases where K_{II} and K_{III} are close to zero, differences of more than 20 % are observed between the predictions, in general, it can be concluded that the predictions made using the equations are close to the analysis predictions.

6. Summary and conclusions

This study attempts the critical issue of mixed-mode fracture behavior in reactor pressure vessels (RPVs) and its implications for structural integrity and safety. Fracture analyses cover a broad spectrum

Table 2
Comparison of mixed mode SIFs obtained for intermediate values of the variables.

β (°)	α (°)	a/c	a/t	FCPAS (MPa $\sqrt{m}$)			Developed eqs. (MPa $\sqrt{m}$)			Difference (%)		
				K_I	K_{II}	K_{III}	K_I	K_{II}	K_{III}	K_I	K_{II}	K_{III}
22.5	52.5	0.625	0.09375	35.90	28.31	−17.08	33.59	24.86	−19.83	6.9	13.9	13.9
52.5	22.5	1	0.0625	19.37	6.90	−20.23	19.51	7.60	−20.68	0.8	9.2	2.2
67.5	22.5	0.75	0.1875	16.26	7.84	−23.70	19.24	10.06	−24.74	15.5	22.1	4.2
22.5	67.5	1.5	0.2185	16.60	27.17	−11.55	15.11	29.13	−15.66	9.8	6.7	26.2
22.5	0	0.625	0.09375	67.00	0.50	−22.04	65.99	0.69	−22.99	1.5	27.7	4.1
52.5	0	1	0.0625	22.40	0.60	−21.33	23.67	0.63	−22.33	5.4	4.9	4.5
67.5	0	0.75	0.1875	21.33	3.61	−23.86	24.86	3.39	−25.28	14.2	6.6	5.6
22.5	0	1.5	0.2185	58.42	1.38	−17.79	60.37	1.47	−20.32	3.2	5.6	12.4
0	22.5	0.625	0.09375	71.26	19.47	−2.22	73.27	19.49	−1.77	2.7	0.1	25.9
0	52.5	1	0.0625	27.58	24.78	−1.33	27.37	25.22	−1.08	0.7	1.7	22.9
0	67.5	0.75	0.1875	32.87	38.88	−3.48	29.15	43.00	−3.65	12.8	9.6	4.6
0	22.5	1.5	0.2185	61.41	21.61	−2.72	67.06	22.03	−2.82	8.4	1.9	3.5

of crack shape aspects and depth ratios and orientations, providing a comprehensive understanding of SIFs along the crack front. Three-dimensional fracture analyses were performed employing enriched finite elements along the crack front using FRAC3D, which is a general-purpose standalone fracture analysis program. The study demonstrates that the influence of these parameters on SIFs is significant. Based on the results of the fracture analyses, some key observations regarding possible crack patterns considered critical to the structural integrity of the reactor pressure vessel and their impact on SIFs are given below;

- Increasing crack depth ratio (a/t) and crack shape aspect ratio (a/c) generally leads to increased SIFs for all K_I, K_{II}, and K_{III} across all angles.
- Cracks with lower β and α angles experience higher SIFs for K_I and potentially significant K_{II} and K_{III} values making them more prone to initiation and growth and may pose a greater threat to the structural integrity of the reactor vessel due to increased susceptibility to fracture.

This study indicates that the orientation of the crack, whether inclined or deflected, plays a crucial role in the distributions of SIFs. In order to make the determination of SIFs practical and easy, regression-based empirical equations are proposed considering the effects of the aforementioned parameters on mixed mode SIFs, K_I, K_{II}, and K_{III}. The developed equation (Eq. 2) for mode-I SIF is shown to be highly reliable, as evidenced by their excellent agreement with reference data from a previous study. The equations developed for mode-II and mode-III SIFs (Eqs. (4) and (5)) were validated by additional fracture analyses performed for various crack configurations. In summary, this study provides detailed analysis information on mixed-mode fracture behavior at the inlet nozzle-cylinder intersection area of RPV and provides engineers with valuable tools to accurately determine SIFs under various crack configurations. These findings are expected to contribute to the overall design, safety, and reliability of critical structures in the nuclear reactor field.

Declaration of competing interest

The authors declare that they have no known competing financial interests or personal relationships that could have appeared to influence the work reported in this paper.

Acknowledgements

The support by Dr. Ali O. Ayhan is gratefully acknowledged for providing FCPAS software.

References

[1] W.L. Server, R.K. Nanstad, Reactor pressure vessel (RPV) design and fabrication: the case of the USA, in: Irradiation Embrittlement of Reactor Pressure Vessels (RPVs) in Nuclear Power Plants, Woodhead Publishing Series in Energy, 2015, pp. 3–25.
[2] P.G. Tipping, Plant life management (PLiM) practices for pressurized light water reactors (PWR), in: P.G. Tipping (Ed.), Understanding and Mitigating Ageing in Nuclear Power Plants, Woodhead Publishing Series in Energy, 2010, pp. 609–632.
[3] R.W. Derby, Shape factors for nozzle-corner cracks, Exp. Mech. 12 (12) (1972) 580–584.
[4] C. Ruiz, Stress intensity factors for nozzle corner cracks, Strain 9 (1) (1973) 7–10.
[5] C.W. Smith, M. Jolles, W.H. Peters, Stress intensities for nozzle cracks in reactor vessels, Exp. Mech. 17 (12) (1977) 449–454.
[6] C.W. Smith, W.H. Peters, W.T. Hardrath, T.S. Fleischman, Stress intensity distributions in nozzle corner cracks of complex geometry, in: Trans. Of the Fifth Int. Conf. on Struct. Mech. in Reactor Tech., 1979. G4/4.
[7] C.W. Smith, W.H. Peters, M.I. Jolles, Stress intensity factors for reactor vessel nozzle cracks, J. Pressure Vessel Technol. 100 (2) (1978) 141–149.
[8] K.N. Akhurst, G.G. Chell, Methods of calculating stress intensity factors for nozzle corner cracks, Int. J. Pres. Ves. Pip. 14 (4) (1983) 227–257.
[9] C. Guozhong, H. Qichao, Approximate stress-intensity factor solutions for nozzle corner cracks, Int. J. Pres. Ves. Pip. 42 (1) (1990) 75–96.
[10] G. Chai, Q. Hong, Stress intensity factors of nozzle corner cracks, Eng. Fract. Mech. 38 (1) (1991) 27–35.
[11] M.A. Mohamed, J. Schroeder, Stress intensity factor solution for crotch-corner cracks of tee-intersections of cylindrical shells, Int. J. Fract. 14 (6) (1978) 605–621.
[12] Z. Gao, L. Xu, K. Zhang, Fatigue crack growth in the nozzle corner of a pressure vessel, Int. J. Pres. Ves. Pip. 42 (1) (1990) 1–13.
[13] T. Jin, Z. He, P. Liu, Z. Wang, Y. Li, D. Wang, A new stress intensity factor solution based on the response surface method for nozzle corner cracks in nuclear reactor for thermal energy generation, Front. Energy Res. 9 (2021) 801919.
[14] W. Schmitt, G. Bartholome, A. Gröstad, M. Miksch, Calculation of stress-intensity factors of cracks in nozzles, Int. J. Fract. 12 (3) (1976) 381–390.
[15] W. Schmitt, Analysis of a crack in a nuclear pressure vessel nozzle using three-dimensional crack tip singularity elements, Int. J. Pres. Ves. Pip. 3 (2) (1975) 123–136.
[16] M.J.G. Broekhoven, Computation of stress intensity factors for nozzle corner cracks by various finite element procedures, in: Third International Conference on Structural Mechanics in Reactor Technology, 1975. G4/6.
[17] D. Aurich, W. Brocks, D. Noack, H. Veith, Elastic-plastic FEM-analysis of a nozzle corner crack and discussion of the results by some fracture mechanics concepts, Nucl. Eng. Des. 72 (1) (1982) 43–52.
[18] W. Brocks, D. Noack, H. Veith, H.-H. Erbe, Elastic-plastic analysis of a nozzle corner crack by finite element method, Int. J. Pres. Ves. Pip. 10 (3) (1982) 219–234.
[19] A. Cella, A. Macchi, C. Sampietri, Fracture mechanics characterization of a 1:5 scale PWR vessel model, Int. J. Pres. Ves. Pip. 40 (4) (1989) 259–278.
[20] Y.R. Rashid, J.D. Gilman, Three-dimensional analysis of reactor pressure vessel nozzles, in: First International Conference on Structural Mechanics in Reactor Technology, 1971. G2/6.
[21] T.K. Hellen, A.R. Dowling, Three-dimensional crack analysis applied to an LWR nozzle-cylinder intersection, Int. J. Pres. Ves. Pip. 3 (1) (1975) 57–74.
[22] S.N. Atluri, B.R. Bass, J.W. Bryson, K. Kathiresan, NOZ-FLAW: A Finite Element Program for Direct Evaluation of Stress Intensity Factors for Pressure Vessel Nozzle-Corner Flaws, 1981.
[23] H. Miyamoto, M. Kikuchi, T. Okazaki, M. Kubo, The J integral evaluation of a nozzle corner crack under thermal transient loading condition, Nucl. Eng. Des. 75 (2) (1983) 213–222.
[24] W.W. Wilkening, 3-D elastic analysis of a circular nozzle corner crack, J. Pressure Vessel Technol. 108 (4) (1986) 474–478.
[25] B. Wang, D. Xu, W. Ye, Y. He, X. Liang, Computation of SIF (stress intensity factor) of corner crack in interior wall of nozzle of nuclear vessel, Int. J. Pres. Ves. Pip. 51 (3) (1992) 349–359.

[26] D. Siegele, L. Hodulak, I. Varfolomeyev, G. Nagel, Failure assessment of RPV nozzle under loss of coolant accident, Nucl. Eng. Des. 193 (3) (1999) 265–272.
[27] A.T. Diamantoudis, G.N. Labeas, Stress intensity factors of semi-elliptical surface cracks in pressure vessels by global-local finite element methodology, Eng. Fract. Mech. 72 (9) (2005) 1299–1312.
[28] U.T. Murtaza, M.J. Hyder, The effects of thermal stresses on the elliptical surface cracks in PWR reactor pressure vessel, Theor. Appl. Fract. Mech. 75 (2015) 124–136.
[29] U.T. Murtaza, M.J. Hyder, Fracture analysis of the set-in nozzle of a PWR reactor pressure vessel-Part 1: determination of critical crack, Eng. Fract. Mech. 192 (2018) 343–361.
[30] Y. Li, T. Jin, Z. Wang, D. Wang, Engineering critical assessment of RPV with nozzle corner cracks under pressurized thermal shocks, Nucl. Eng. Technol. 52 (11) (2020) 2638–2651.
[31] V.F. González-Albuixech, G. Qian, M. Sharabi, M. Niffenegger, B. Niceno, N. Lafferty, Coupled RELAP5, 3D CFD and FEM analysis of postulated cracks in RPVs subjected to PTS loading, Nucl. Eng. Des. 297 (2016) 111–122.
[32] T. Zhang, F.W. Brust, G. Wilkowski, D.L. Rudland, A. Csontos, Welding residual stress and multiple flaw evaluation for reactor pressure vessel head replacement welds with alloy 52, ASME Pressure Vessels and Piping Conference 43697 (2009) 577–586.
[33] B. Spencer, M. Backman, P. Chakraborty, W. Hoffman, Reactor Pressure Vessel Fracture Analysis Capabilities in Grizzly, 2015.
[34] R. Liu, M. Huang, Y. Peng, H. Wen, J. Huang, C. Ruan, H. Ma, Q. Li, Analysis for crack growth regularities in the nozzle-cylinder intersection area of Reactor Pressure Vessel, Ann. Nucl. Energy 112 (2018) 779–793.
[35] K. Liu, M. Huang, J. Lin, H. Jiang, B. Wang, H. Matsuda, The effects of thermal stress on the crack propagation in AP1000 reactor pressure vessel, Theor. Appl. Fract. Mech. 110 (2020) 102798.
[36] O. Demir, A.O. Ayhan, S. İriç, A new specimen for mixed mode-I/II fracture tests: modeling , experiments and criteria development, Eng. Fract. Mech. 178 (2017) 457–476.
[37] O. Demir, A.O. Ayhan, H. Lekesiz, in: Investigation of Mixed Mode - I/II Fracture Problems - Part 1: Computational and Experimental Analyses 35, 2016, pp. 330–339.
[38] O. Demir, A.O. Ayhan, Investigation of mixed mode-I/II fracture problems - Part 2: evaluation and development of mixed mode-I/II fracture criteria 35 (2016) 340–349.
[39] A.O. Ayhan, O. Demir, A novel test system for mixed mode-I/II/III fracture tests – Part 1 : modeling and numerical analyses, Eng. Fract. Mech. 218 (2019) 106597. April.
[40] O. Demir, A.O. Ayhan, S. İriç, A novel test system for mixed mode-I/II/III fracture tests – Part 2: experiments and criterion development, Eng. Fract. Mech. 220 (2019) 106671.
[41] M.F. Yaren, O. Demir, A.O. Ayhan, S. Iriç, Three-dimensional mode-I/III fatigue crack propagation: computational modeling and experiments, Int. J. Fatig. 121 (2019) 124–134.
[42] ANSYS, Theory Manual Version 12.0, Ansys Inc.", Canonsburg, PA, USA, 2009.
[43] A.O. Ayhan, H.F. Nied, FRAC3D-Finite element based software for 3-D and generalized plane strain fracture analysis, Semiconductor Research Corporation (SRC) (1998). Technical Report.
[44] A.O. Ayhan, H.F. Nied, Stress intensity factors for three-dimensional surface cracks using enriched finite elements, Int. J. Numer. Methods Eng. 54 (6) (2002) 899–921.
[45] A.O. Ayhan, Mixed mode stress intensity factors for deflected and inclined surface cracks in finite-thickness plates, Eng. Fract. Mech. 71 (7–8) (2004) 1059–1079.
[46] AP1000 Design Control Document, U.S. Nuclear Regulatory Commission. Reactor Coolant System and Connected Systems, Revision 19 Tier 2. Westinghouse (Chapter vol. 5, Section 5.3 Reactor Vessel).
[47] Q. Du, G.Y. Shi, Efficient analysis of 3D mixed-mode cracks of a pressure vessel based on schwartz-neuman alternating method, Appl. Mech. Mater. 853 (2017) 266–271.
[48] Minitab Inc. Minitab Software for Quality Improvement. Version vol. 18.